In situ OBSERVATION USING A SCANNING TUNNELING MICROSCOPE OF A LOCAL MORPHOLOGICAL LIGHT-INDUCED TRANSFORMATION OF n-MOLYBDENUMDISULFIDE IN CONTACT WITH ACETONITRILE CONTAINING A SMALL AMOUNT OF WATER

Kenji SAKAMAKI*, Kohichiroh HINOKUMA and Akira FUJISHIMA

Department of Synthetic Chemistry, Faculty of Engineering, The University of Tokyo, 7-3-1, Hongo, Bunkyo-ku, Tokyo, 113, Japan

Received April 18, 1990
Accepted August 24, 1990

Dedicated to the memory of Prof. J. Heyrovský on the occasion of his centenary.

A scanning tunneling microscope (STM) under photoelectrochemical control was used to expand the understanding of nanometer scale in situ photoelectrochemical processes at an n-MoS_2/acetonitrile interface. A local morphological light-induced transformation occurred around a MoS_2(0001) surface depression. This morphological transformation was attributed to the n-MoS_2 photoelectrochemical reaction which was controlled by a small amount of water contained in the acetonitrile. After visible light illumination (276 s), photoelectrochemical reactions under anodic polarization transformed the original depression into a "right-angled triangular" type depression.

Two-dimensionally layered transition metal chalcogenides are attractive materials owing to their physical diversities which arise due to the existence of *d* bands and the degree of their filling[1,2]. 2H-MoS_2 is perhaps the most representative material since it is the only compound which is found in appreciable quantities in nature, and also because it is employed both as a catalyst and as a dry lubricant in industrial processes. MoS_2 has the unique characteristics of being a diamagnetic semiconductor in its filled, non-bonding d_{z^2} state[3], and also its structure is highly anisotropic. Tributsch and Bennett[4-6] were the first to investigate n-MoS_2 photoelectrochemical reactions for use in solar energy conversion applications, however in the absence of effective redox systems, photoanodic corrosion is the dominant process. Light-induced MoS_2 photodecomposition processes have been studied by electrochemical techniques[7-13], light (optical) microscopy[11], scanning electron microscopy (SEM)[11,12], and scanning

* All correspondence concerning this paper should be addressed to: Kenji Sakamaki, c/o Prof. Dr Allen J. Bard, Department of Chemistry, The University of Texas at Austin, Texas, 78712-1167 (Fax: 512-471-0088, Phone: 512-471-3761).

electron microscope energy dispersive X-ray analysis (SEM-EDX)[11]. The topography of cleaved/oxidized MoS_2 surfaces has also been investigated[14,15] from a solid state physics viewpoint by using optical microscopy and the SEM. Research performed from a surface chemistry perspective is very important to expand the understanding of photocorrosion processes, and therefore a scanning tunneling microscope (STM) under potentiostatic control has become a promising method for in situ characterization of electrode surfaces[16–22]. Recently much attention has been focused on observing semiconductor/solution interfaces[23–26], however reports of in situ photoelectrochemical studies on a layer-type semiconductor electrode using the STM under potentiostatic control have not been published, and led to the presented report's study of the photoelectrochemical processes of n-MoS_2. Investigations have been conducted of in situ photoelectrochemical processes at the n-MoS_2 electrode surface in KCl[27], KI[27], acetonitrile (CH_3CN) + H_2O (4 vol. %)[28], and, CH_3CN + KI (4 vol. %)[29]. In the presented paper an in situ STM technique is applied to photoelectrochemically studied MoS_2 in CH_3CN, and attention is focused on the effects of MoS_2's structural anisotropy on the photoelectrochemical reactions taking place in a CH_3CN solution containing a small amount of H_2O, thereby allowing localized photo-oxidation phenomena to be investigated.

EXPERIMENTAL

The electrochemical STM tunneling unit consisted of a StandAlone (SA) microscope (Digital Instruments, Inc., U.S.A.) and a locally manufactured electrochemical cell which were previously described[28]. The SA microscope was connected to both a Nanoscope II microscope control unit and a locally manufactured bipotentiostat. The main advantages of the electrochemical tunnel unit was that in situ electrochemical STM measurements could be performed in organic solutions, as well as aqueous solutions, by controlling the potential of the working electrode (E_W) against a saturated calomel reference electrode (SCE). The STM measurements under potentiostatic control were carried out using the four electrode system shown in Fig. 1. The potential of the tip (E_T) with respect to the SCE is given by $E_T = E_W - T_B$ (V vs SCE), where T_B is the tunnel bias voltage (working electrode (WE)/tip (ground)). The total current when imaging in a constant

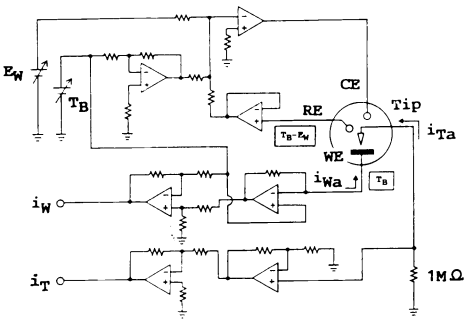

FIG. 1
An electrical schematic of the four-electrode system used

current mode is the summation of the real tunneling current and the background current. To gain realiable STM images a background current must be detected, therefore an electronic method was developed for determining the background current using the bipotentiostatic control shown in Fig. 1. Prior to taking STM measurements, the background current at the tip was detected separately from the tunneling region while controlling the potential of both the tip and the WE, thus characterizing the tip conditions that occurred. After measuring the background current and examining the tip condition in order to apply suitable electrode potentials to both the WE and the tip for STM imaging, the in situ measurements were performed. The 2H-MoS_2 single crystals (n-type) were natural minerals, with the donor concentration of MoS_2 being calculated by using the Mott–Schottky relationship ($1{\cdot}3 \cdot 10^{18}$ cm^{-3})[10]. Fresh MoS_2(0001) surfaces were prepared by cleaving with Scotch tape just before STM measurements. Satisfactory electrical contact was achieved by applying a Ga-In eutectic to the backside of the freshly cleaved surfaces. A spectrograde CH_3CN solvent ($H_2O < 0{\cdot}1$ vol. %) and a guaranteed reagent tetra-n--butylammonium perchlorate (TBAP) supporting electrolyte were used. Insulated $Pt_{0.8}Ir_{0.2}$ tips (30 MΩ) were used for measurements in solutions, with their electrochemical properties being discussed in Sakamaki et al.[30]. To provide insulation from the solvent's vapors, the tube-type piezoelectric scanner was covered with a room temperature drying silicone. The entire n-MoS_2 surface (exposed area: $0{\cdot}126$ cm^2) in the electrochemical cell was illuminated by an optical fiber guided 30 W halogen lamp. The time evolution of the STM images under photoelectrochemical control was recorded by six imaging buffers contained in the computer workstation of Nanoscope II microscope.

RESULTS AND DISCUSSION

Figure 2 shows STM top-view images of an n-MoS_2(0001) 500 × 500 nm surface in CH_3CN/$1 \cdot 10^{-2}$M-TBAP. Figures 2a, b, and c were respectively observed 0 s, 138 s, and 276 s after visible light illumination. The measurements were conducted in the constant current mode ($7{\cdot}3$ nA) at $T_B = +0{\cdot}5$ V, $E_W = +0{\cdot}5$ V vs SCE, and $E_T = 0$ V vs SCE. The flat-band and the conduction band edge potentials of n-MoS_2 in CH_3CN were respectively $+0{\cdot}30$ V and $+0{\cdot}20$ V vs SCE[31], with electron tunneling occurring at these potential conditions from the tip to the n-MoS_2 conduction band. The value of $E_w = +0{\cdot}5$ V vs SCE was chosen to avoid an ordinary anodic decomposition of n-MoS_2, and also to keep the current low while in the dark, with the photocurrent density at this potential being $\sim 79{\cdot}4$ μA cm^{-2}. Background current was less than $0{\cdot}02$ nA and increased during the experiments due to the presence of photoelectrochemical reaction products such as soluble corrosion species, yet still was rather low in comparison with measurements made in a $1 \cdot 10^{-3}$M-KCl aqueous solution[27]. Figure 2a shows the initially occurring surface defects, vacancies, and depressions, with the formations denoted as P1, P2, P3, P4, and P5. An almost identical profile was observed 276 s after visible light illumination (Fig. 2c), thus it is concluded that the well-ordered (0001) crystal face was stable against photoelectrochemical reactions in the CH_3CN solvent. However, using closer more accurate observations, photooxidation and photocorrosion reactions were seen to gradually proceed around the large P1 depression, and also a new pit (P6) was formed below

P1 as shown in Figs 2b and c. It is quite apparent that P1's shape was morphologically transformed, and therefore the structural changes around P1 were magnified in Figs 3a, b, and c, which respectively show the three-dimensional (3D) magnified STM images of Figs 2a, b, and c. A more definitive structure can now be seen on the well-ordered (0001) MoS_2 surface in Fig. 3a, and the morphological transformation processes at P1 are shown in Figs 3b and c, i.e., P1's shape clearly changes into a "right-angled triangular" shape. These morphological transformations, which occurred on a nanometer scale at the n-MoS_2/CH_3CN interface, were attributed to the n-MoS_2 photoelectrochemical reactions which were controlled by the small amount of H_2O contained in the CH_3CN solvent. Evidence supporting the existence of anisotropically enhanced photoelectrochemical reactions around surface depressions and vacancies by adding H_2O (4 vol. %) to CH_3CN/1 . 10^{-2}M-TBAP has been reported in Sakamaki et al.[28], and although the spectrograde CH_3CN solvent had H_2O of less than 0·1 vol. %, additional H_2O could have possibly been absorbed from air into the solvent. The small amount of H_2O contained in CH_3CN appears to be a significant factor in nanometer scale morphological surface transformations because

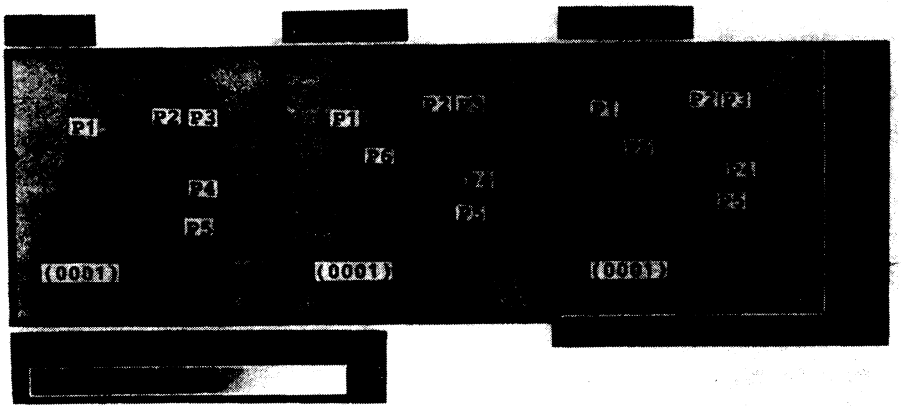

FIG. 2

In situ STM top-view images of n-MoS_2(0001) in CH_3CN/1 . 10^{-2}M-TBAP under photoelectrochemical control. All images were taken over an area of 500 × 500 nm in a constant current mode (7·3 nA) at $E_W = +0{\cdot}5$ V and $E_T = 0$ V vs SCE. Figures a, b, and c were respectively observed at 0 s, 136 s, and 276 s after visible light illumination

it induced local photoelectrochemical oxidation reactions around the depressions, and also made it possible to observe for a long time the nanometer scale transformations occurring at the well-ordered undistorted $MoS_2(0001)$ face, which was obviously stable against photooxidation, being in fair agreement with the results of Kautek and Gerischer[11].

Light-induced n-MoS_2 photoanodic reactions in an inert electrolyte are generally assumed to follow one of the below reactions:

$$MoS_2 + 8H_2O + 18h^+ \rightarrow Mo^{6+} + 2SO_4^{2-} + 16H^+ \qquad (1)$$

$$MoS_2 + 2H_2O + 4h^+ \rightarrow MoS_2 + O_2 + 4H^+ , \qquad (2)$$

where h^+ represents photo-generated holes. Equation (*1*) was the predominant reaction in this study, with sulfate being the main product of the photoelectrochemical oxidation of MoS_2[6,10]. The photoelectrochemical reaction of Eq. (*2*) appears to occur at the undistorted surface which has vacant octahedral holes in every alternate layer (Fig. 4). Tributsch[4,5] reported that the initial oxygen production proceeded at a freshly prepared MoS_2-van der Waals' surface, and that this oxygen was then consumed as a reactive sulfate production intermediate. However, Figs 2 and 3 show that the photoelectrochemical reaction (Eq. (*1*)) predominantly occurred at the surface defects, depressions, and vacancies because these sites have "dangling

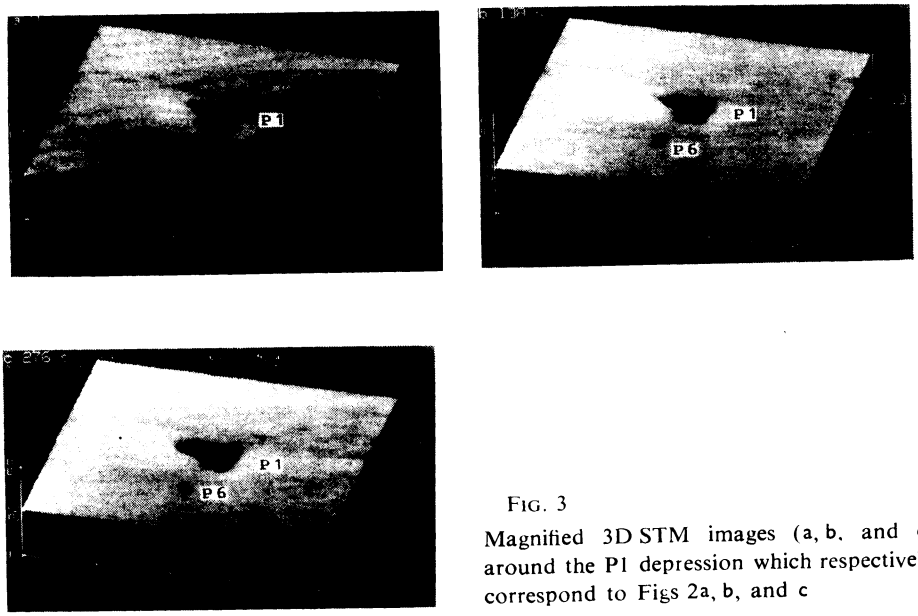

FIG. 3

Magnified 3D STM images (a, b, and c) around the P1 depression which respectively correspond to Figs 2a, b, and c

bonds" which make them more active when compared with the van der Waals' surface. The formation of P6 is attributed to photoelectrochemical dissolution at impurity sites, which is highly probable since the n-MoS_2 single crystal used was a natural mineral. Although the n-MoS_2 impurity level was not quantified in this study, impurities are known to exist in Japanese samples as reported by Frindt and Yoffe[32] (Si 0·1 ~ 1%), Al 0·1%, Fe 0·01 ~ 0·1%, and Cu, Pb, Sn, Bi, Mg 0·001 ~ ~ 0·01%). Attention is not focused on this possible impurity result, but instead on the photoelectrochemically morphological transformations around P1 with respect to the crystallographic MoS_2 structure. The 2H(hexagonal)-MoS_2 with trigonal prism coordination (D_{3h}) consists of S—Mo—S "sandwiched" layers along the *c*-axis by weak van der Waals forces, with the *c*-axis stacking sequence in the unit cell shown in Fig. 4. After visible light illumination (276 s) the initial P1 depression (Fig. 3a) was morphologically transformed into a "right-angled triangular" type depression (Fig. 3c) following an intermediate surface profile shown in Fig. 3b. The length of the hypotenuse of this depression, lying in the $[11\bar{2}0]$ direction, was 78 nm, with the base and leg of the triangle being respectively oriented in the $[2\bar{1}\bar{1}0]$ and $[01\bar{1}0]$ directions. Figure 4 is shown to clarify which bonds were broken by the local photoelectrochemical reaction. The precision of the crystallographic orientation of the "right-angled triangular" depression was experimentally assured by verifying that the atomic patterns were separated by 0·32 nm in the MoS_2 basal plane, i.e., the (0001) crystal face was observed on the cleaved surface by the STM. The OH^- ions and radicals are able to attack bare Mo^{4+} sites in the depressions, yet due to a structural hindrance it is not easy for the OH^- ions to attack the Mo^{4+} sites in

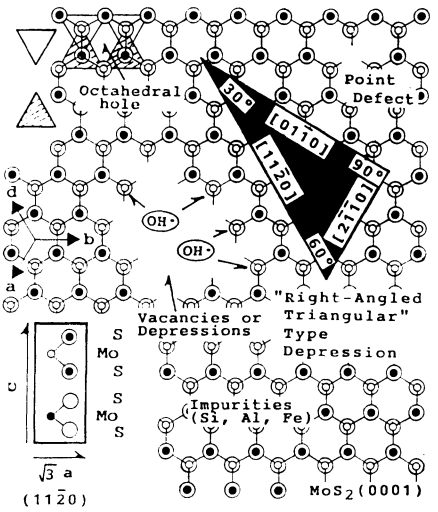

FIG. 4

Schematic representation of the 2H-MoS_2(0001) face, a cross-section through (11$\bar{2}$0), a point defect, vacancies, depressions, and the "right-angled triangular" type depression

the well-ordered layers because these ions must penetrate from the *c*-axis direction through the vacant octahedral holes in every alternate layer (Fig. 4), and therefore the photoelectrochemical reactions proceed predominantly at the surface defects, depressions, vacancies, and impurities sites.

CONCLUSION

The STM under photoelectrochemical control was used to investigate in situ photoelectrochemical reactions at the n-MoS_2 semiconductor electrode in CH_3CN containing a small amount of H_2O. Although the well-ordered (0001) face was found to be stable against the photocorrosion in CH_3CN, photocorrosion did occur at surface depressions, vacancies, and pits, all of which served as active reaction sites. Local morphological transformations which occurred on a nanometer scale at the n-MoS_2/CH_3CN interface were attributed to the n-MoS_2 photoelectrochemical reactions which were controlled by the small amount of water contained in the CH_3CN solvent. Photoelectrochemical reactions transformed the original surface depression into a "right-angled triangular" type depression.

Thanks are given to Prof. H. Tributsch, Prof. R. Memming, and Prof. R. Tenne for their fruitful discussions. Additional thanks are extended to Prof. Y. Gohshi, Prof. K. Itoh, Prof. K. Itaya for their beneficial suggestions during the initial STM *research phase.*

REFERENCES

1. Wilson J. A., Yoffe A. D.: Adv. Phys. *18*, 193 (1969).
2. Yoffe A. D.: Chem. Soc. Rev. *5*, 51 (1976).
3. Bell G., Liang W. L.: Adv. Phys. *25*, 53 (1976).
4. Tributsch H.: Z. Naturforsch., A *32*, 972 (1977).
5. Tributsch H.: Ber. Bunsenges. Phys. Chem. *81*, 361 (1977).
6. Tributsch H., Bennett J. C.: J. Electroanal. Chem. Interfacial Electrochem. *81*, 97 (1977).
7. Kautek W., Gerischer H., Tributsch H.: Ber. Bunsenges. Phys. Chem. *83*, 1000 (1979).
8. Kautek W., Gerischer H.: Ber. Bunsenges. Phys. Chem. *84*, 645 (1980).
9. Kautek W., Gerischer H., Tributsch H.: J. Electrochem. Soc. *127*, 2471 (1980).
10. Fujishima A., Noguchi Y., Honda K., Loo B. H.: Bull. Chem. Soc. Jpn. *55*, 17 (1982).
11. Kautek W., Gerischer H.: Surf. Sci. *119*, 46 (1982).
12. Ahmed S. M., Gerischer H.: Electrochim. Acta *24*, 705 (1979).
13. Ahmed S. M.: Electrochim. Acta *27*, 707 (1982).
14. Thomas J. M., Evans E. L.: Nature *214*, 167 (1967).
15. Bahl O. P., Evans E. L., Thomas J. M.: Proc. R. Soc. London, A *306*, 53 (1968).
16. Lustenberger P., Roher H., Cristoh R., Siegenthaler H.: J. Electroanal. Chem. Interfacial, Electrochem. *243*, 225 (1988).
17. Wiechers J., Twomey T., Kolb D. M., Behm R. J.: J. Electroanal. Chem. Interficial Electrochem. *248*, 451 (1988).
18. Bard A. J., Fan F. R., Kwak J., Liv O.: Anal. Chem. *61*, 132 (1989).
19. Itaya K., Sugawara S., Sashikata K., Furuya N.: J. Vac. Sci. Technol., A *8*, 515 (1990).
20. Uosaki K., Kita H.: J. Electroanal. Chem. Interfacial Electrochem. *259*, 301 (1989).

21. Yau S.-L., Viyus C. M., Schardt B. C.: J. Am. Chem. Soc. *112*, 3677 (1990).
22. Sakamaki K., Itoh K., Fujishima A., Gohshi Y.: J. Vac. Sci. Technol., A *8*, 525 (1990).
23. Itaya K., Tomita E.: Chem. Lett. *1989*, 285; Surf. Sci. *219*, L515 (1989).
24. Lin C. W., Fan F. R., Bard A. J.: J. Electrochem. Soc. *134*, 1038 (1987).
25. Thundat T., Nagahara L. A., Lindsay S. M.: J. Vac. Sci. Technol., A *8*, 539 (1990).
26. Uosaki K., Fukuda M., Kita H.: Denki Kagaku *57*, 1213 (1989).
27. Sakamaki K., Hinokuma K., Fujishima A.: J. Vac. Sci. Technol., submitted.
28. Sakamaki K., Hinokuma K., Hashimoto K., Fujishima A.: Surf. Sci., Lett. *237*, L 383 (1990).
29. Hinokuma K., Sakamaki K., Fujishima A.: Bull. Chem. Soc. Jpn. *63*, 2713 (1990).
30. Sakamaki K., Itoh K., Fujishima K., Gohshi Y., Nakagawa H.: Bull. Chem. Soc. Jpn. *62*, 2890 (1989).
31. Schneemèyer L. F., Wrighton M. S.: J. Am. Chem. Soc. *101*, 6496 (1979).
32. Frindt R. F., Yoffe A. D.: Proc. R. Soc. London., A *273*, 69 (1962).